DFT calculations of vacancy formation energies and interaction energies with hydrogen atoms in tungsten

Daiji Kato

National Institute for Fusion Science

Dept. Fusion Science, SOKENDAI

contents

- Introduction
- DFT calculations of vacancy and di-vacancy formation energies
- H-V complex formation in W and its effects on void nucleation and hydrogen retention
- Summary

Fusion power output ～3GW
DT fusion reaction ～ a few %

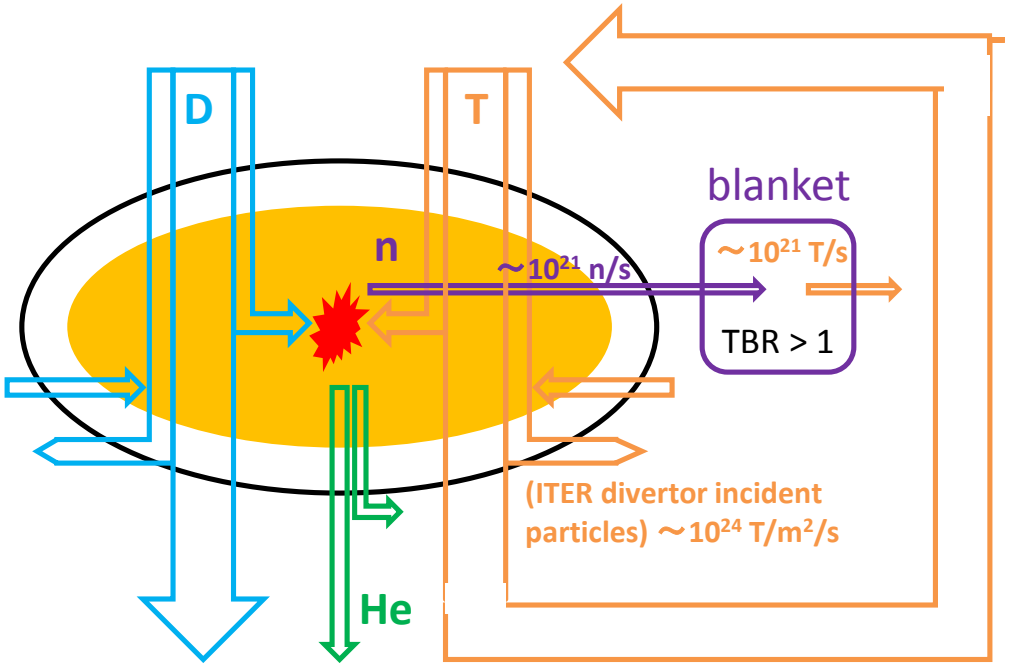

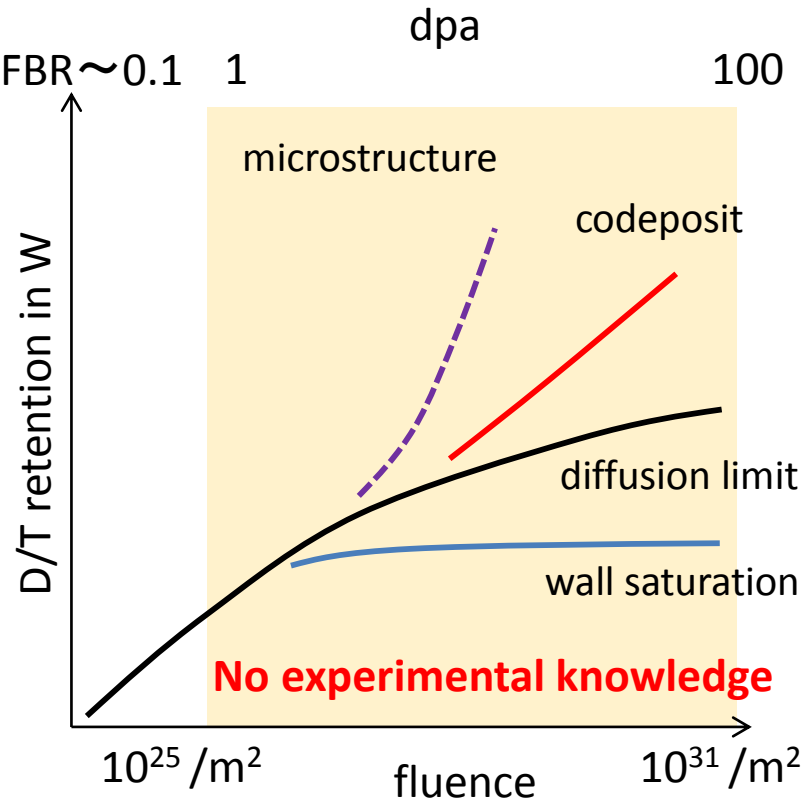

- T invetory increase (Wall pumping)
  - thermal diffusion deep and trapped inside (square root of incident fluence)
  - codeposition with sputtered particles (low T, linearly increase with fluence)
  - microstructure develop (T dependence ?, fluence dependence ?)
- Reemission character ⇒ Optimal operation temperature window

Introduction

- Radiation damage effects on tritium retention in the tungsten divertor is a key issue for full-W option.

– **BULK/ Primary roles of n-induced radiation damage (e.g., vacancy and dislocation loop):**
D plasma exposure ($2x10^{18}D/m^2/s$, $6x10^{22}D/m^2$, 473K) to a damaged tungsten specimen by fission neutron (HFIR, 0.025 and 0.3dpa@373K) leads to a large enhancement (about 1 %) of D concentration over a few micron depth.
W surrogate ion (MeV) damage leads to a large increase of D retention.

– **SURFACE/ High-flux divertor plasma effects (e.g., blistering):**
Higher flux irradiation leads to a significant enhancement of D retention [e.g. Alimov, 2008].
D+C ion-driven permeation experiments suggested super-saturated D in tungsten [Peng, Ueda, 2013].

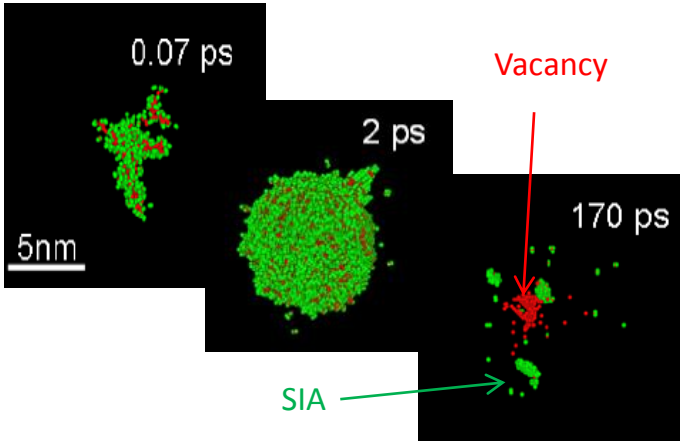

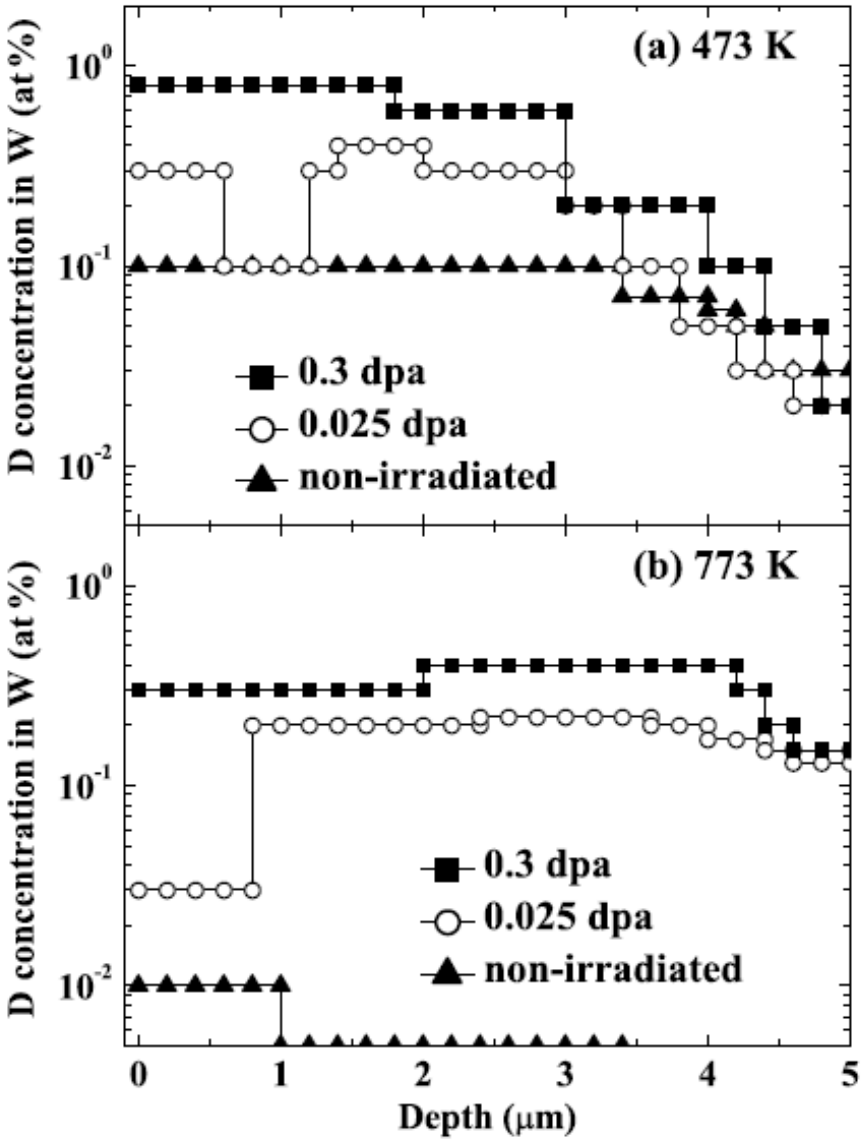

Figure 2. Depth profiles of D in non-irradiated and n-irradiated W specimens (0.025 and 0.3 dpa) after exposure to D plasma at 473 K (*a*) and 773 K (*b*).

Hatano Y. et al 2013 Nucl. Fusion 53 073006

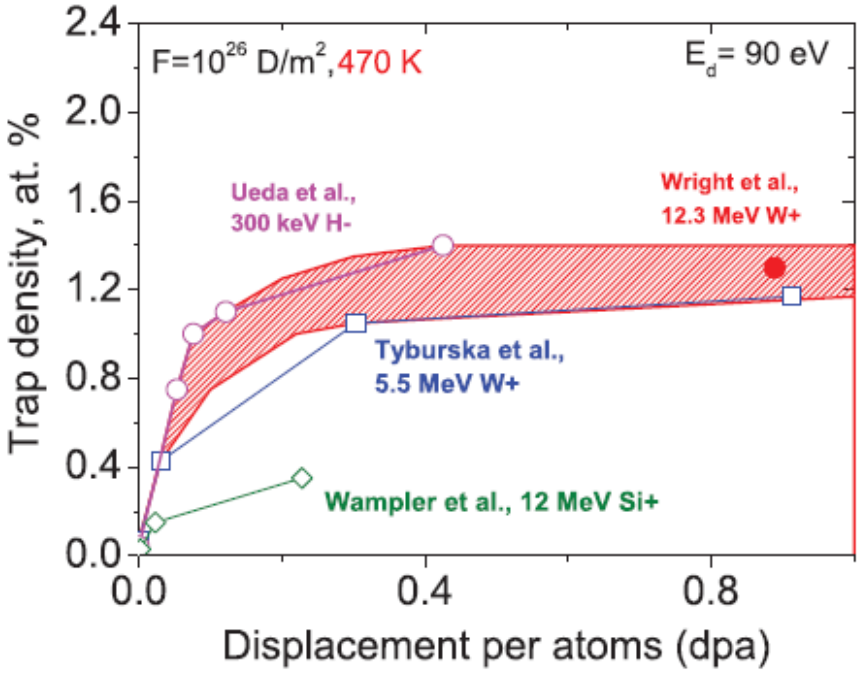

Figure 7. Dependence of hydrogen trap density in W as function of dpa induced by irradiation with different high energy heavy ions [55].

Roth J. and Schmid K. 2011 Phys. Scr. T145 014031

D trap concentration in damaged W

Surrogate ion experiments

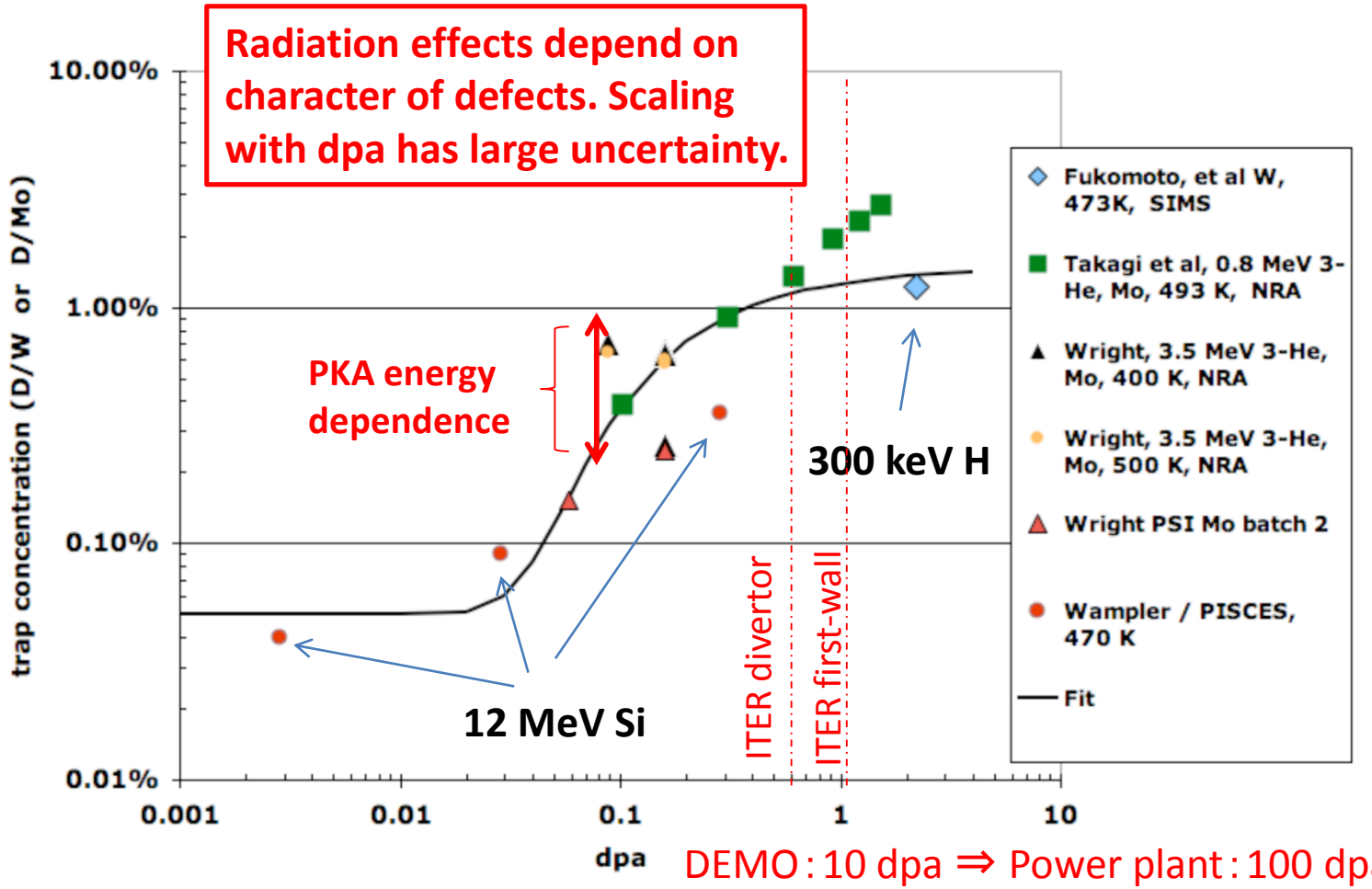

DEMO : 10 dpa ⇒ Power plant : 100 dpa

$$\text{Traps / W} = 6\times10^{-4} + 1.4\times10^{-2}\exp(-0.15/\text{dpa})$$

Whyte, ITPA (2008) **Ueda (Osaka Univ.)**

Super-saturated D and blistering (D/C mixed irradiation)

Temperature dependence of D/W fraction at the ion range

$$C_R - C_b \sim \phi_p d/D$$

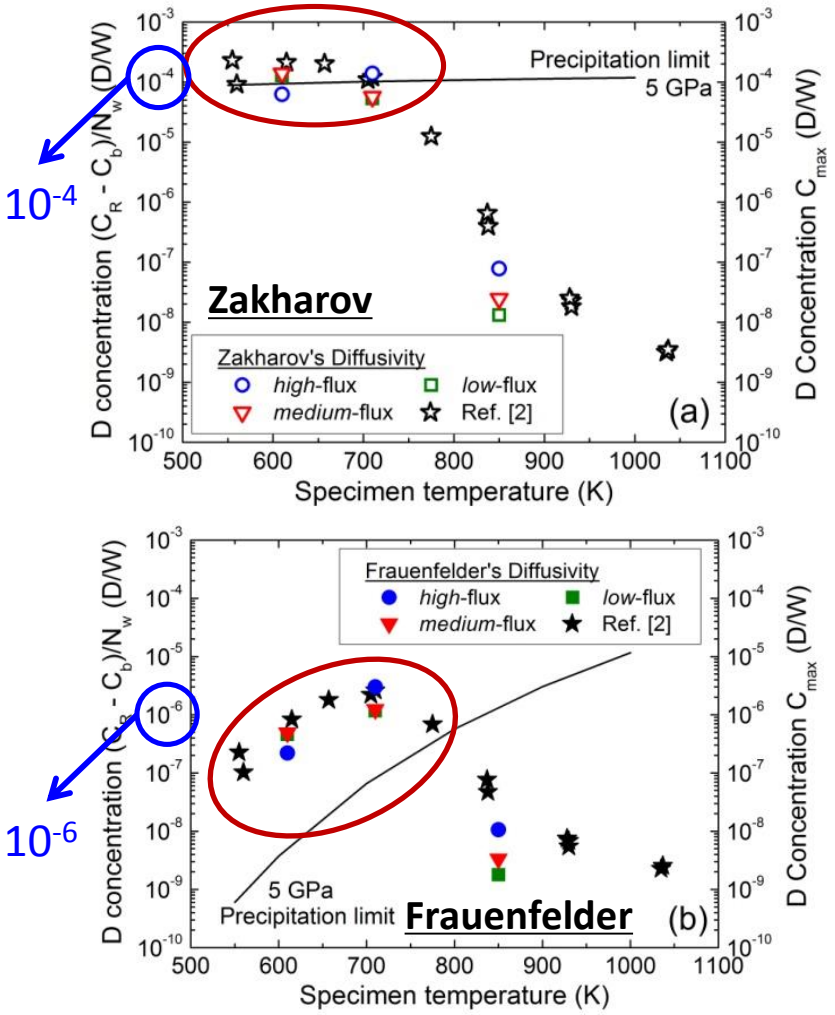

Peng H.Y. et al 2013 J. Nucl. Mater. 438 S1063

D/C mixed irradiation increase D concentration

Blistering on W surfaces by D/C mixed irradiation (f_C=0.7-2.1%). (No blistering observed with D only)

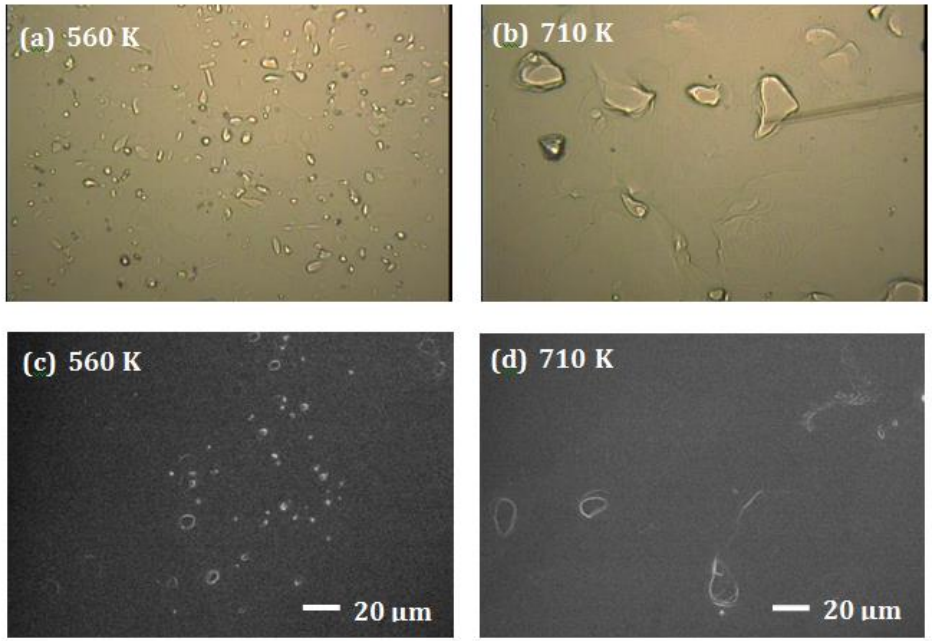

upper) optical microscope image
lower) SEM image

Super-saturation of H concentration by high-flux plasma irradiation

Fractional concentration of H at the surface is estimated in steady state of incident flux $\varphi_{in} = 10^{24}$ /m^2/s.

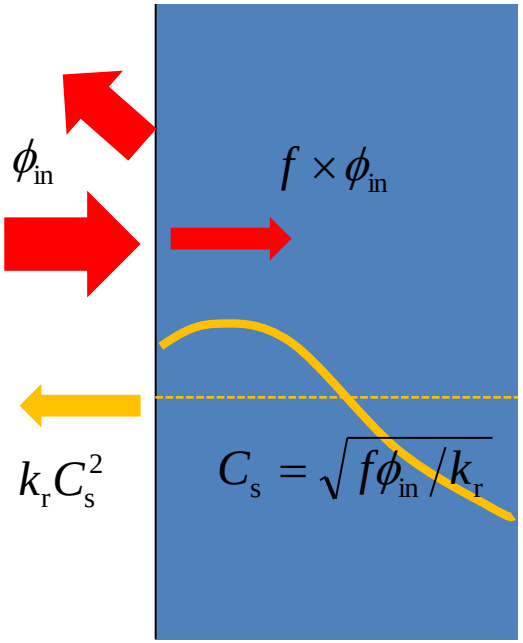

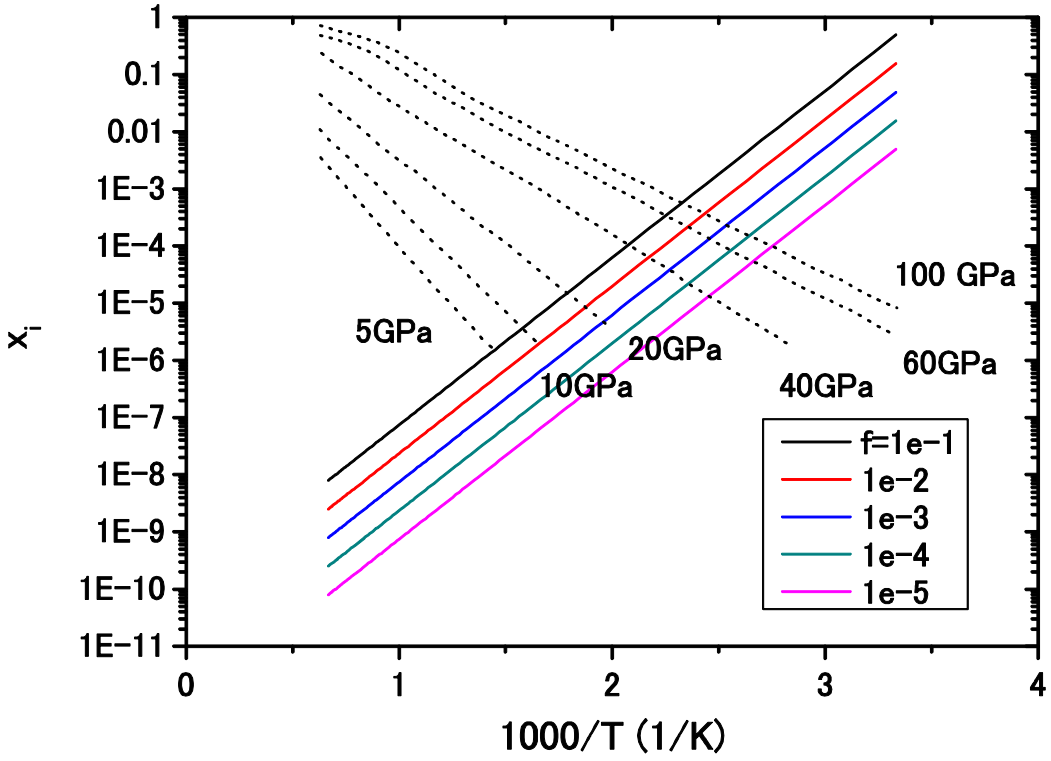

- Anderl's data (Fus. Tech. v.21, 745, 1992) for recombination coefficients k_r, 1 keV D^+ ion, Frauenfelder's diffusivity is used.
- Reflection coefficient (TRIM.SP) 0.76～0.98@10 eV (f=1e-1～1e-2); t'Hoen et al. PRL 111, 2013, f = 1e-5～1e-7@5 eV.
- H solubility in W under high H pressure calculated by Sugimoto&Fukai (Acta Metall. Mater. v.40, 2327, 1992)

Divertor plasma exposure experiment at Large Helical Device (LHD)

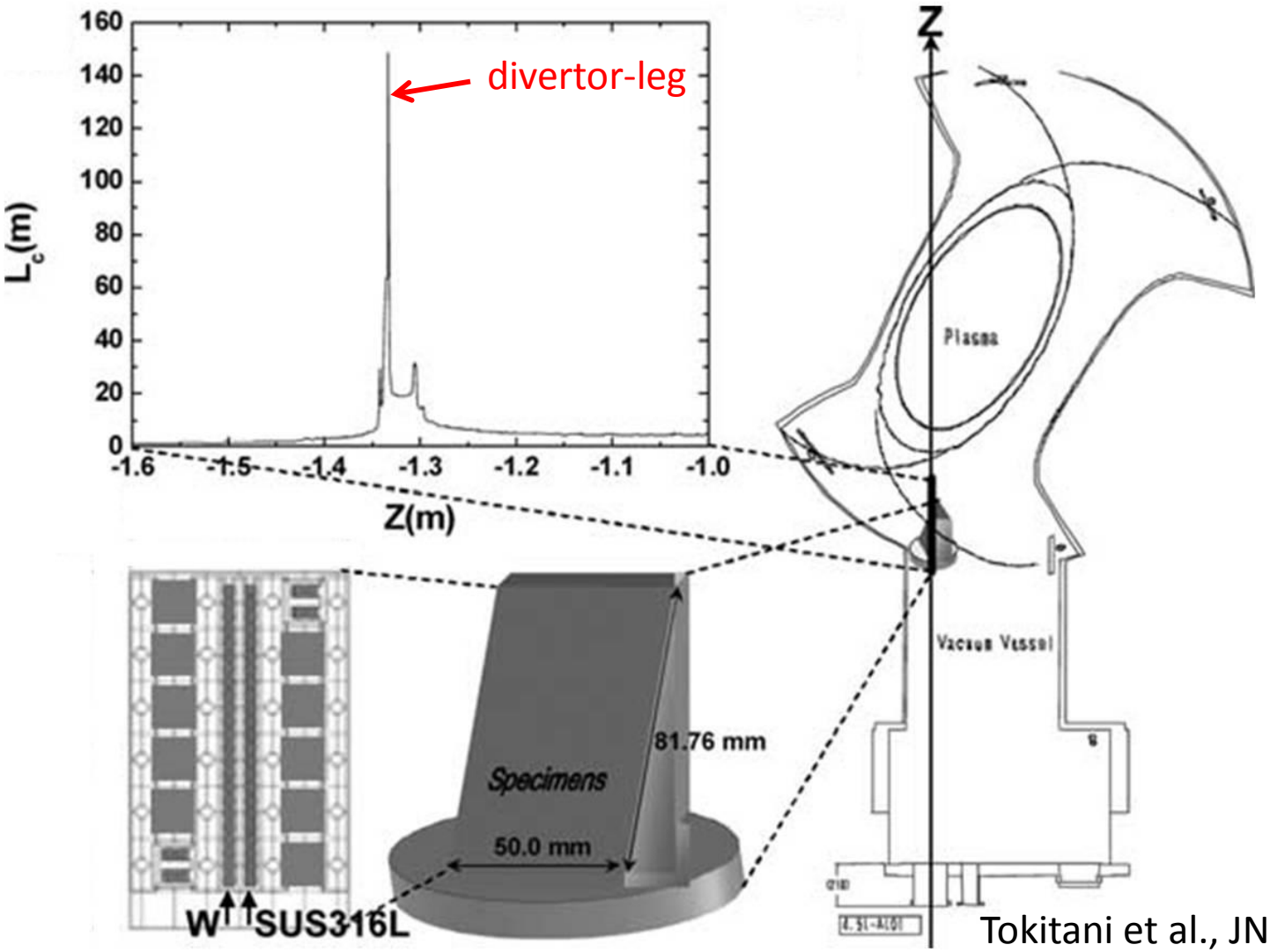

Tokitani et al., JNM (2005)

Nano-cavity in W observed after high-flux hydrogen plasma exposure

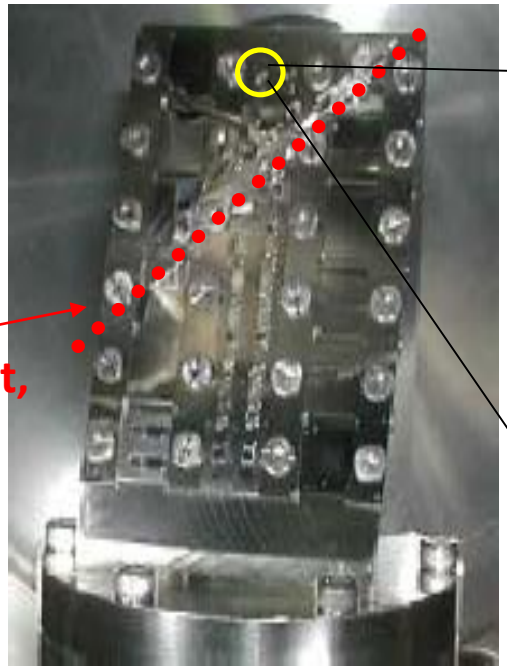

TEM image

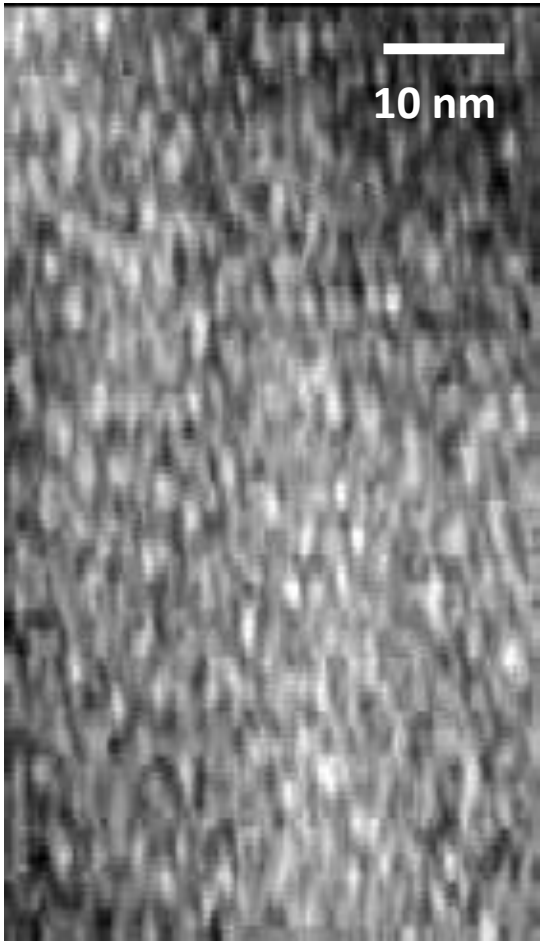

- Discharge time : 26s (19 shots)
- n_e (core) = 2.3 – 4.0x10^{19} /m^3
- T_i (core) = 2.1 – 3.4 keV
- T_e=T_i (divertor) = 10 – 20 eV
- Ion energy on W target: 100 – 200 eV
- Ion particle flux : 10^{22} H/m^2s (Langmuir probe)

Total energy calculation in DFT

$$E = \sum_{n} \int_{\Omega_{BZ}} d^3k \varepsilon_{n\vec{k}} f\left(\frac{\varepsilon_F - \varepsilon_{n\vec{k}}}{\sigma}\right) + E^H[\rho] + E^{xc}[\rho] + \int d^3r V_{loc}^{ion}(\vec{r})\rho(\vec{r}) + E_{Ewald}\left(\{\vec{R}\}\right)$$

$$\int_{\Omega_{BZ}} d^3k \varepsilon_{n\vec{k}} f\left(\frac{\varepsilon_F - \varepsilon_{n\vec{k}}}{\sigma}\right) \approx \sum_{\Omega_{BZ}} \omega_{\vec{k}} \varepsilon_{n\vec{k}} f\left(\frac{\varepsilon_F - \varepsilon_{n\vec{k}}}{\sigma}\right)$$

$$f(x) = \frac{1}{2}(1 - \mathrm{erf}(x)) + A_1 H_1(x) e^{-x^2}$$

(Methfessel and Paxton)

Kresse G. and Furthmüller J. 1996 Phys. Rev. B 54 11169

Convergence of mono-vacancy formation energy in W_{128}

k-point	E(W_{128}) in eV	E($W_{127}V$) in eV	E_f(V) in eV
4x4x4	-1664.9194	-1648.6293	3.282
6x6x6	-1664.8066	-1648.6540	3.146
8x8x8	-1664.7713	-1648.6298	3.135
10x10x10	-1664.7561	-1648.6240	3.126
12x12x12	-1664.7531	-1648.6261	3.121

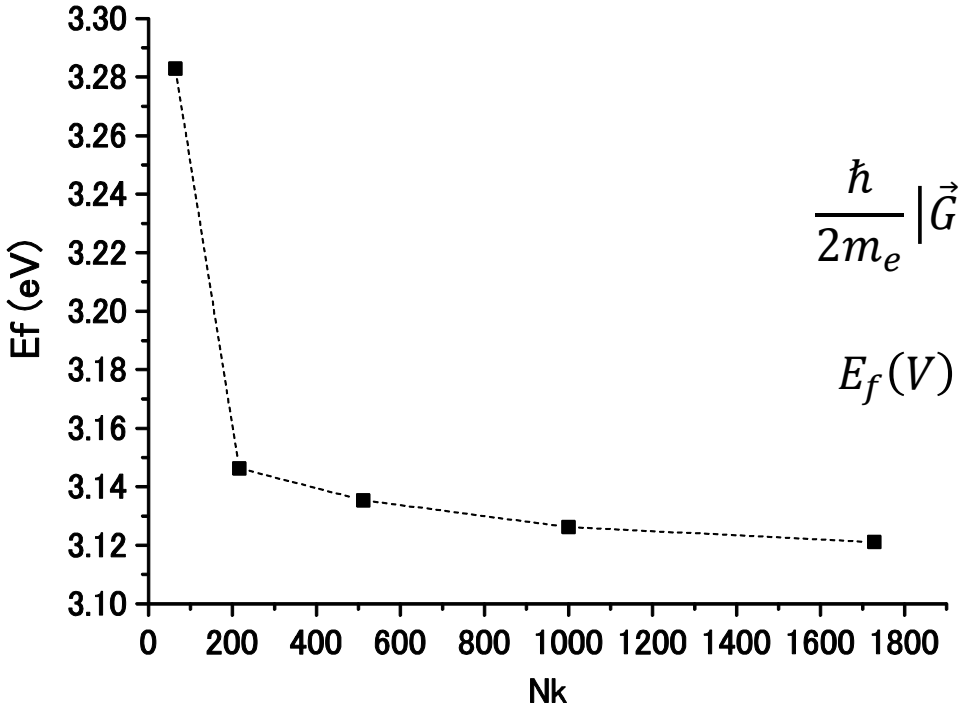

Calculated using VASP v4.6.34 (GGA-PBE)

$$a = 3.165\text{Å},$$

$$\frac{\hbar}{2m_e}\left|\vec{G}+\vec{k}\right|^2 < 223.1eV, \sigma = 0.2eV$$

$$E_f(V) = E(W_{127}V) - \frac{127}{128}E(W_{128})$$

Surface-energy correction of vacancy formation energy in W

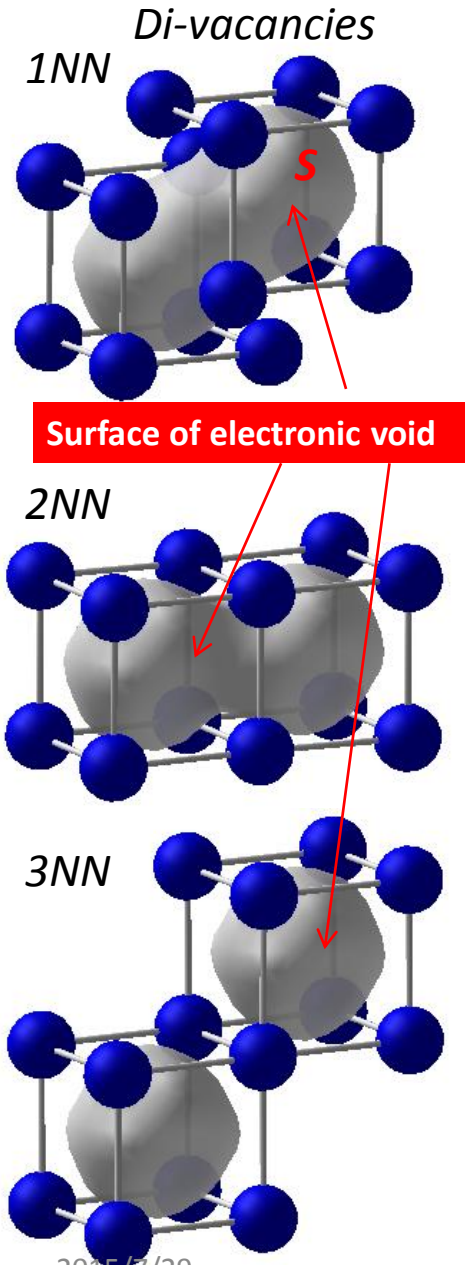

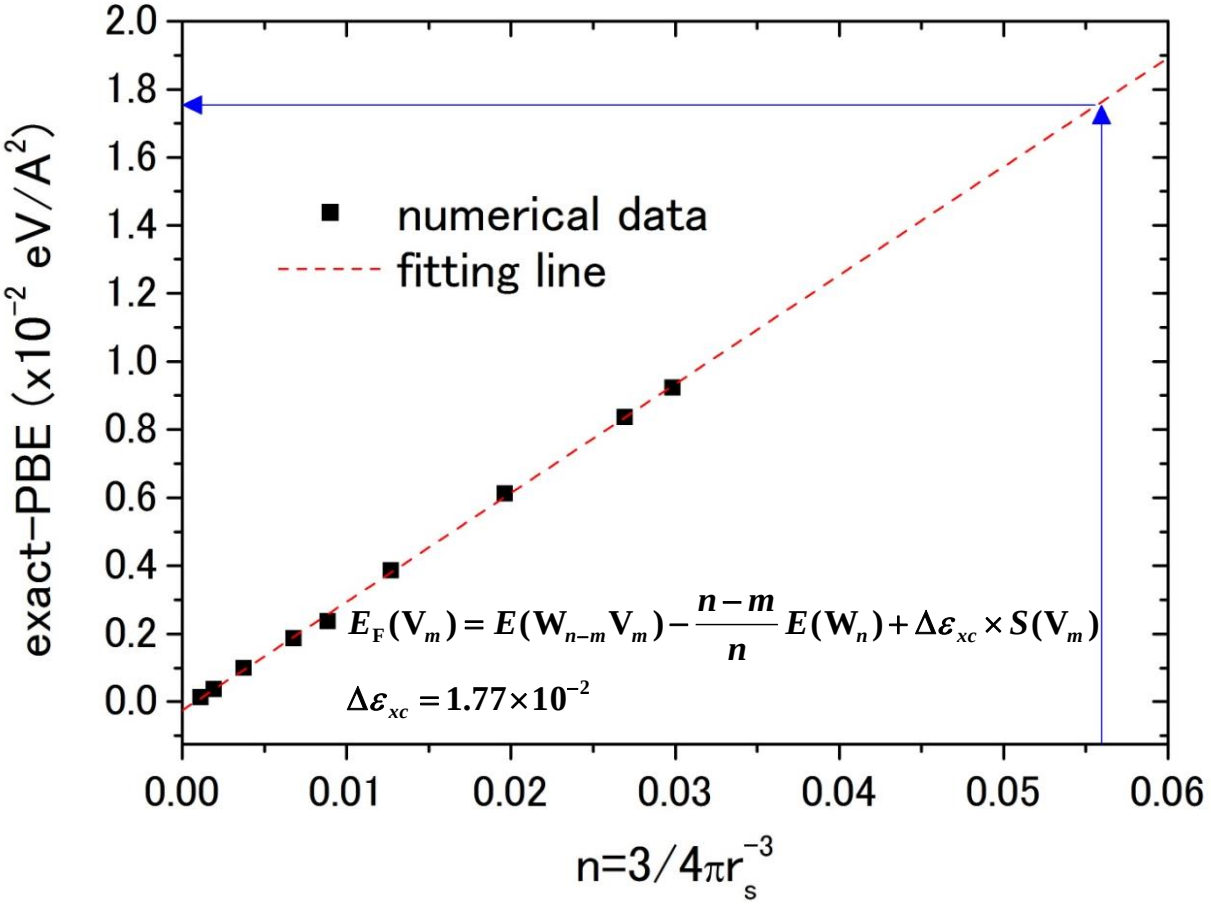

Numerical data for jellium model [S. Kurth, J. P. Perdew, P. Blaha, Int. J. Quantum Chem. 75 (1999) 889.] are adopted; 1.77×10^{-2} eV/Å^2 for Wigner-Seitz radius r_s=1.62 corresponding to an electron density of bulk W.

DFT results of vacancy formation energies in W

	E_F (eV)	Ω_F (Å^3)	B (GPa)	E_B (eV)
Perfect	—	**15.9**	**304**	—
		16.0[b]	305[b]	
		15.8[f]	323[f]	
V_1	**3.68(3.17)**	**10.5**	**309**	—
	3.5–4.1[a]			
	3.56[b]			
	3.6[c]	12.4[c]		
	3.95[e]			
	3.568[h]			
V_2(1NN)	**7.31(6.50)**	**21.4**	**298**	**+0.05(-0.16)**
	6.71[b]			+0.41[b]
	7.06[c]	25.4[c]		+0.14[c]
				+0.7[d]
	7.32[e]			+0.58[e]
				+0.45[g]
	7.129[h]			+0.007[h]
V_2(2NN)	**7.63(6.81)**	**20.1**	**294**	**-0.27(-0.47)**
	6.93[b]			+0.19[b]
	6.42[c]	23.6[c]		+0.78[c]
	7.36[e]			+0.54[e]
				+0.29[g]
	7.325[h]			-0.19[h]
V_2(3NN)	**7.48(6.47)**	**20.8**	**301**	**-0.12(-0.13)**
	7.32[c]	24.8[c]		-0.12[c]

TABLE:
Formation energy (E_F), equilibrium atomic volume, defect formation volume (Ω_F), bulk modulus (B), and binding energy (E_B).
Perfect: perfect crystal, V_1: mono-vacancy, V_2(1NN): first nearrest-neighbor di-vacancy, V_2(2NN): second, and V_2(3NN): third. Bold numbers are present DFT results .

a. Recommended values in Landolt-Börnstein
b. DFT-GGA with package of linear combination of atomic type orbitals (PLATO)
c. Johnson's model potential
d. Experimental data of field ion microscopy
e. Modified embedded atom model calculation
f. Recommended values in Kittle's text
g. Tight-binding basis calculation
h. VASP PBE-AM05

Hydrogen trapping effect on di-vacancy formation in W

V_2H complex binds with H stronger than VH

A nucleus of larger vacancy clusters

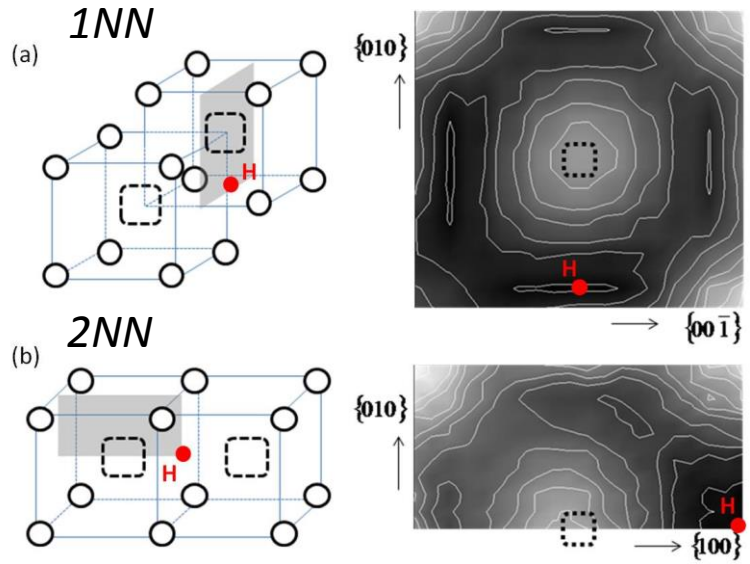

DFT potential energy surface of H

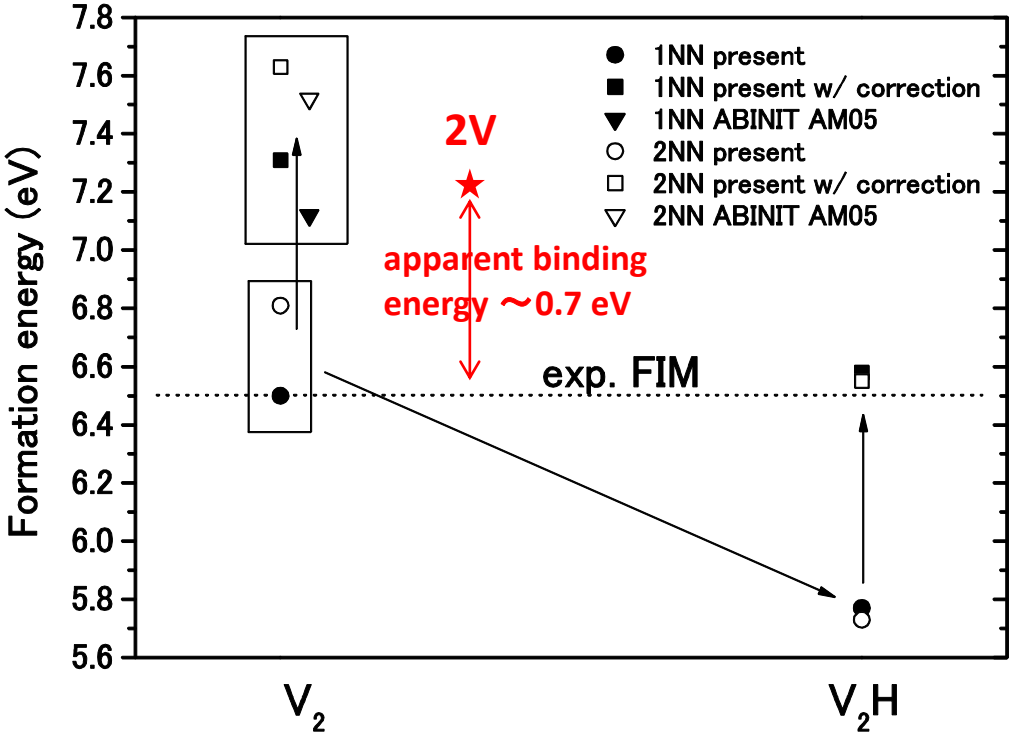

Binding energy of single hydrogen atom to V_2

- 1.8 eV for 1NN at an octahedral site.
- 2.1 eV for 2NN at the center of a line connecting two vacancies.

(Binding energy to V is 1.4 eV)

Hydrogen effect in formation energies of V_2 and V_2H in tungsten for 1NN and 2NN configurations. Other DFT results (triangles, L.Ventelon 2012) using AM05 functional optimized to vacancy calculations are also plotted for comparison. Dotted line indicates an experimental value obtained by field ion microscopy (FIM, J.Y.Park 1983).

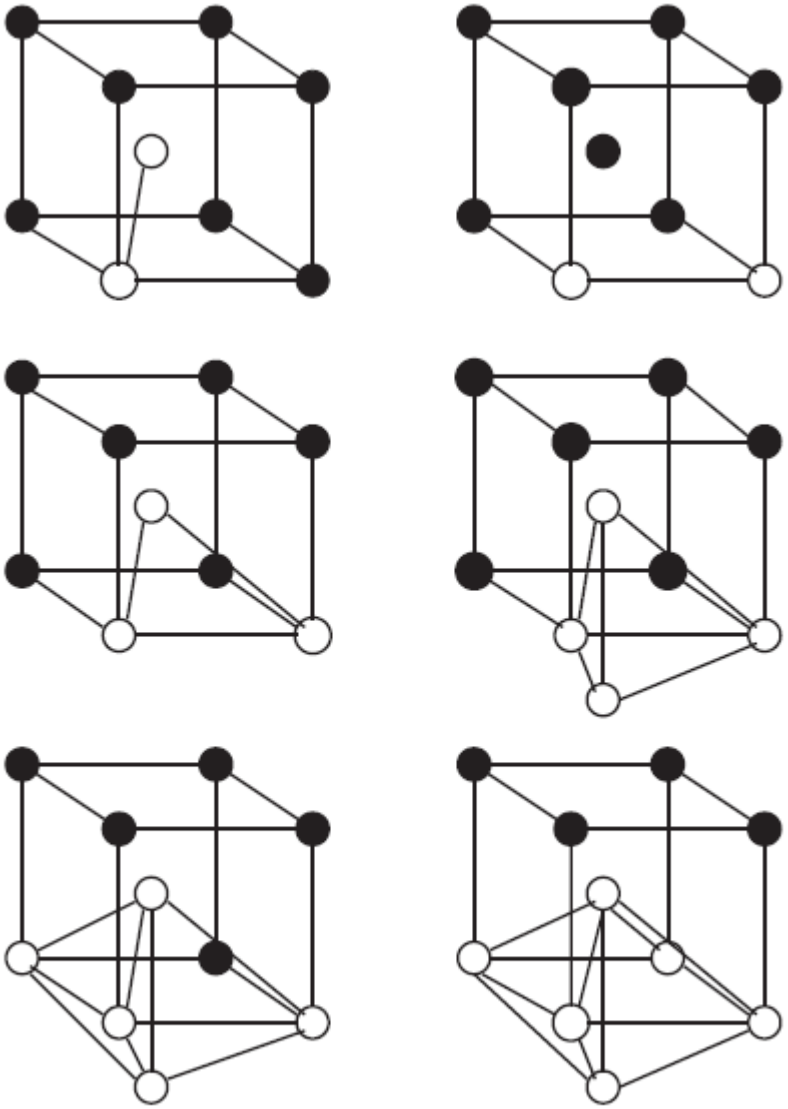

FIG. 12. Tungsten vacancy cluster configurations ($N_v = 2-6$) investigated in the present study.

TABLE III. Formation energies (E_f) and binding energies (E_b), in eV, of vacancy clusters in tungsten. Positive values of the binding energy indicate attraction between the vacancies, leading to clustering of vacancies, whereas negative values indicate repulsion.

Cluster	PBE E_f	PBE-AM05 E_f	PBE E_b	PBE-AM05 E_b
1	3.327	3.568		
2 (⟨111⟩)	6.624	7.129	0.029	0.007
2 (⟨100⟩)	6.989	7.325	−0.365	−0.190
3	9.711	10.454	0.269	0.250
4	12.242	13.398	1.065	0.874
5	14.669	16.103	1.965	1.736
5 (Ref. 71)	15.744	17.230	0.890	0.610
6	17.847	19.457	2.113	1.950

M. Muzyk, D. Nguyen-Manh, K. J. Kurzydłowski, N. L. Baluc, and S. L. Dudarev, PRB 84, 104115 (2011)

D. Kato et al. Nucl. Fusion 55 (2015) 083019

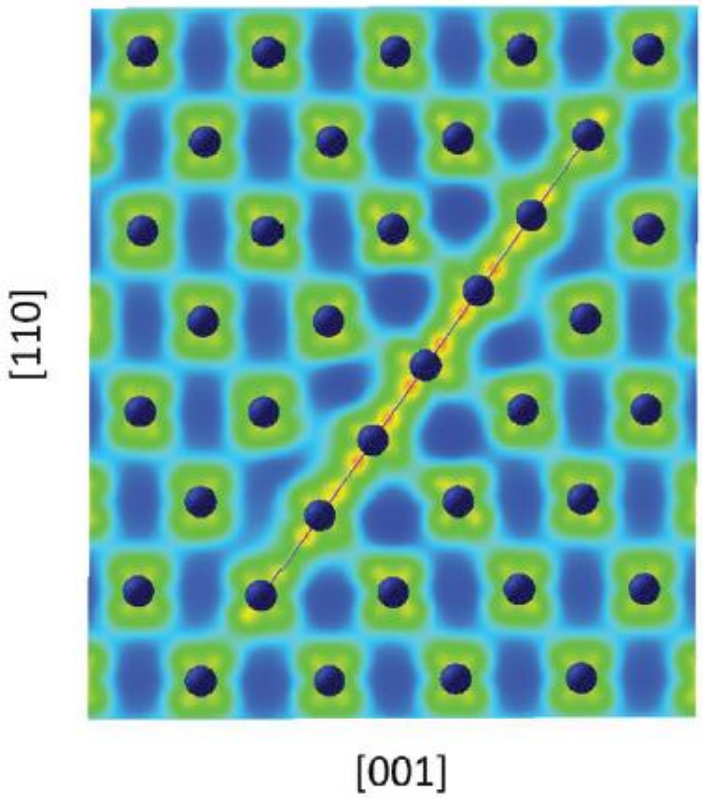

Figure 4. Atomic configuration and electron charge density of 1 1 1-crowdion. Blue balls are tungsten atoms. The crowdion is indicated by an array of bonded atoms along the [1 1 1] direction. Colors on the surface indicate electron densities; red indicates higher electron densities while blue indicates depletion of the electron density.

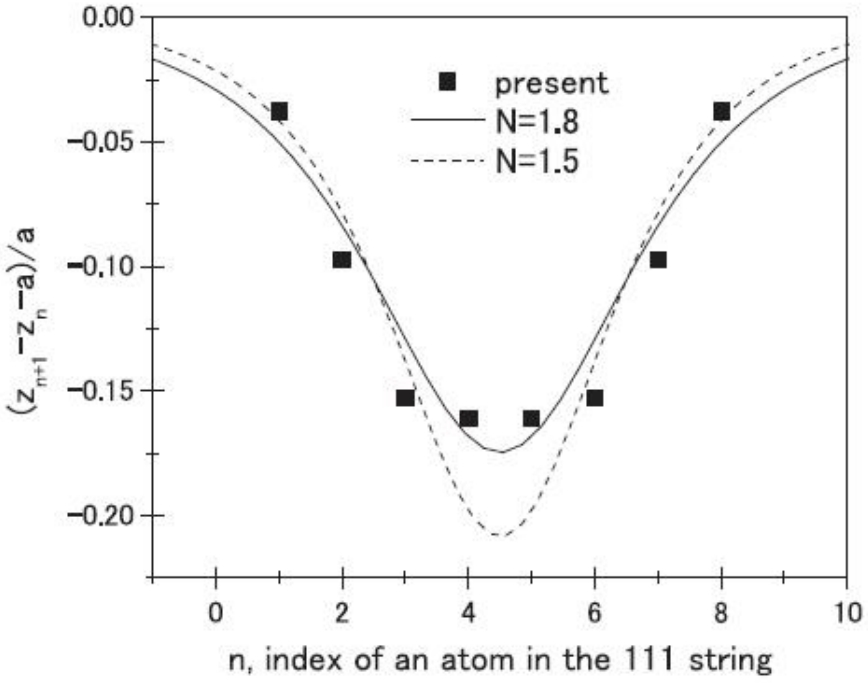

Figure 5. Field of atomic displacements in the 1 1 1-crowdion. Solid squares are present DFT results and curves single-string Frenkel–Kontorova model (equation (5)) assuming $n_0 = 5$.

$$u_n \equiv z_n - na$$
$$\approx \frac{2a}{\pi}\arctan\left[\exp\left(-\frac{n-n_0}{N}\right)\right], \quad u_n \ll Na.$$

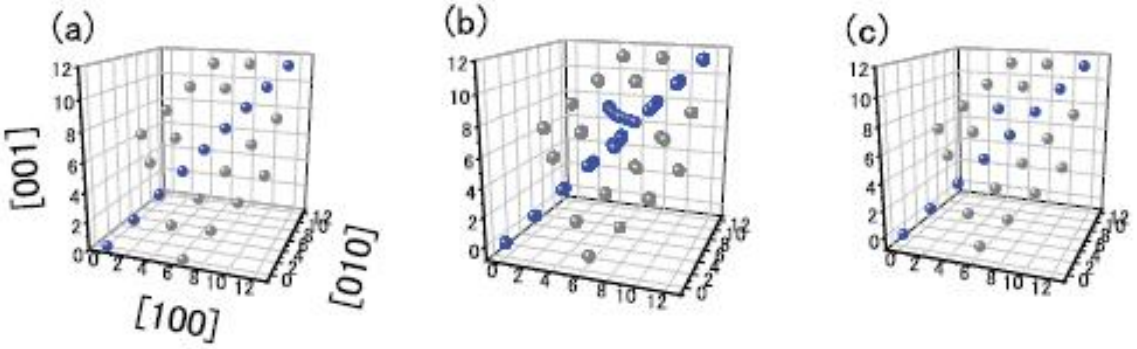

Figure 6. Atomic configurations for recombining mono-vacancy and 1 1 1-crowdion. Blue balls are atoms initially belonging to the central string of the 1 1 1-crowdion, light grey atoms in the first- and second-nearest 1 1 1-strings on the (1 1 0) surface. (*a*) Initial configuration, (*b*) image of configurational relaxation by the conjugate-cradient method, and (*c*) equilibrium (perfect crystal).

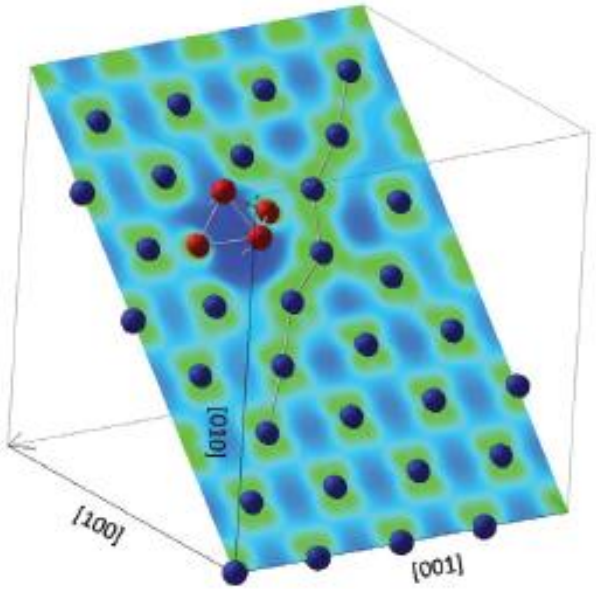

Figure 7. Octahedron hydrogen cluster stacking with a vacancy (VH_6) preventing it from recombining with a 1 1 1-crowdion SIA in tungsten. Blue balls are tungsten and red balls hydrogen atoms, respectively. Tungsten atoms only on (1 1 0) surface are drawn in the figure. Another two hydrogen atoms of VH_6 are behind the surface. The crowdion structure distorted by the presence of VH_6 is indicated by a connected bond.

$$e_f(\mathrm{VH_6 + SIA}) = E(\mathrm{W}_{n-1}\mathrm{VH_6 + SIA}) - E(\mathrm{W}_n) - 3 \times E(\mathrm{H_2}).$$

The formation energy is 12.1 eV which is 0.6 eV smaller than sum of the individual formation energies for the VH6 complex and the 111-crowdion. This indicates that the VH6 complexes can trap the 111-crowdion. Stability of the metastable state at elevated temperatures should be investigated in future studies.

D. Kato et al. Nucl. Fusion 55 (2015) 083019

HxVy complex — Nucleus of void formation under hydrogen-rich condition

The HxVy complex blocks V-I recombination. H_xV_y complex may be responsible for ion-driven trap and hydrogen retention.

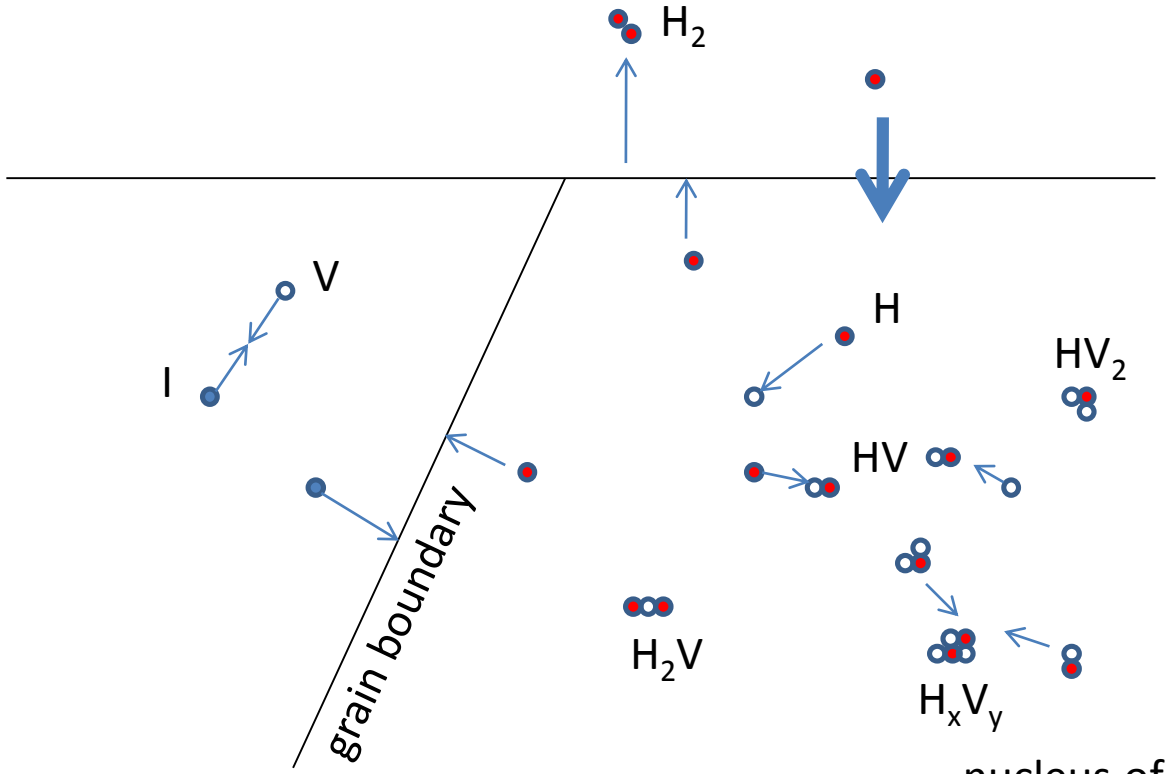

nucleus of void formation

ref. Condon and Schober, JNM 207 (1993)

Typical thermal desorption spectra of D+ irradiate W

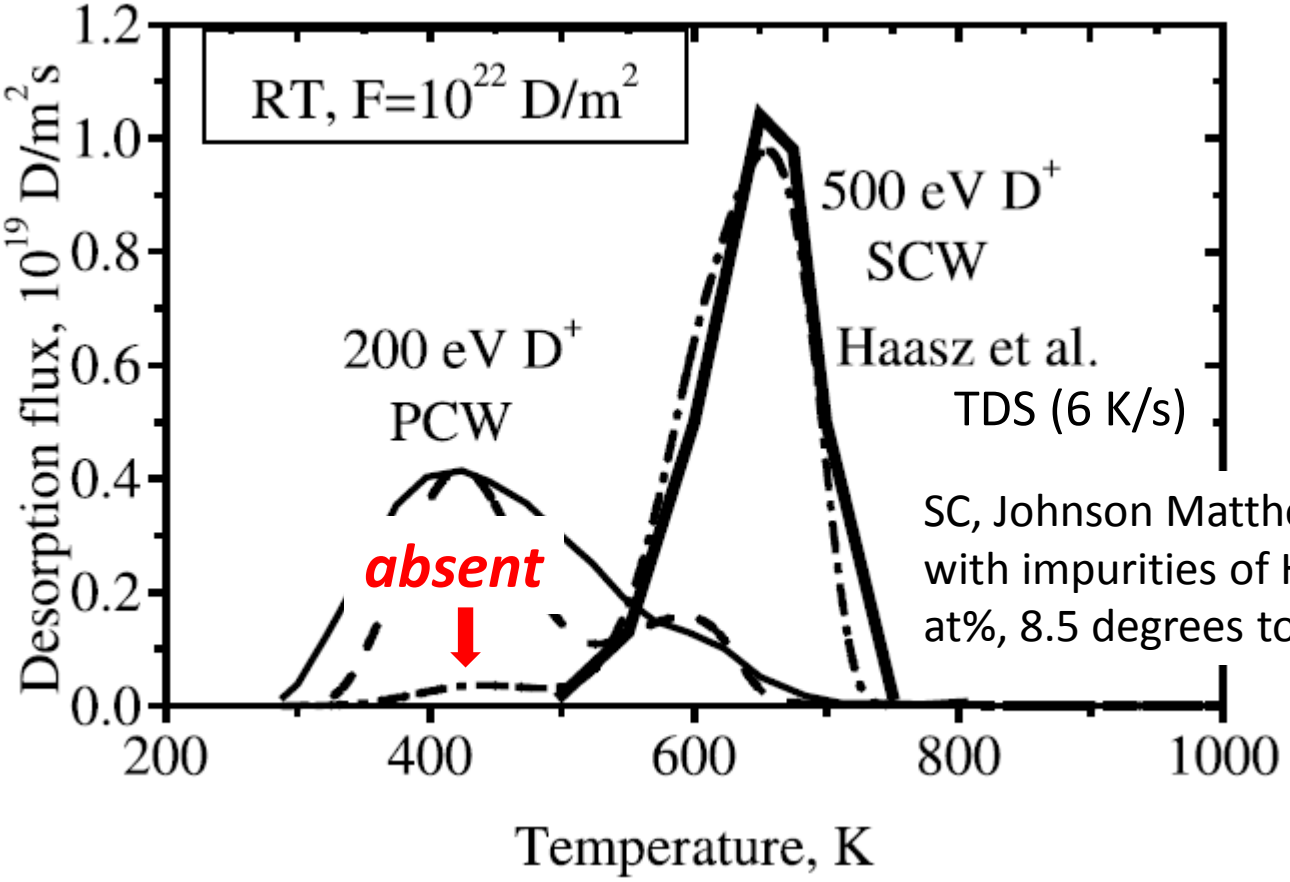

SC, Johnson Matthey, 99.9wt% pure with impurities of H-0.1, C-0.5, O-0.5 at%, 8.5 degrees to [001] plane

Ogorodnikova et al., JNM 313-316 (2003)

DFT potential energy surface of H in W and Minimum Energy Path (MEP) of H desorption from vH

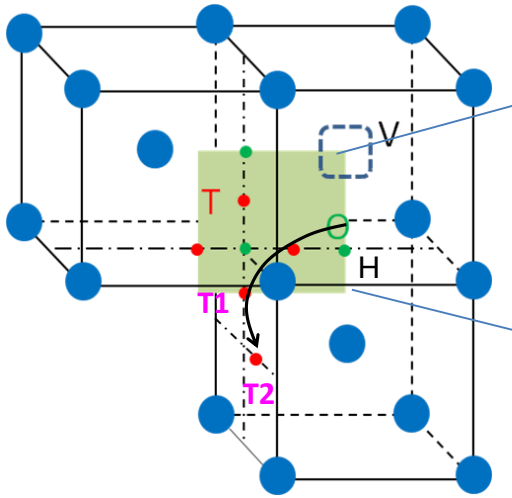

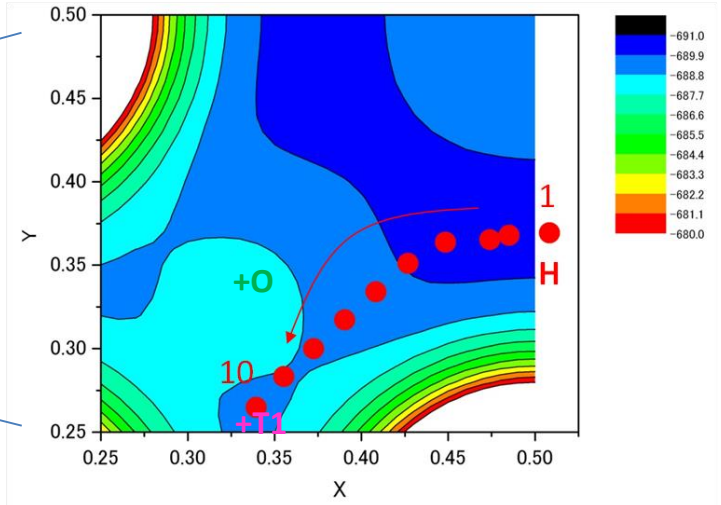

Equilibrium sites of H

- **in vacancy: O site (octahedral)**
- **in matrix: T site (tetrahedral)**

※ desorption path: O → T1 → T2

Transition states (TS1 and TS2) on the MEP. Solid circle is each image of NEB calculations. An intermediate transition state (TS1) is associated with a meta-stable T site (T1). H weakly trapped in a shallow potential well of the T1 site can be easily recombined with vacancy.

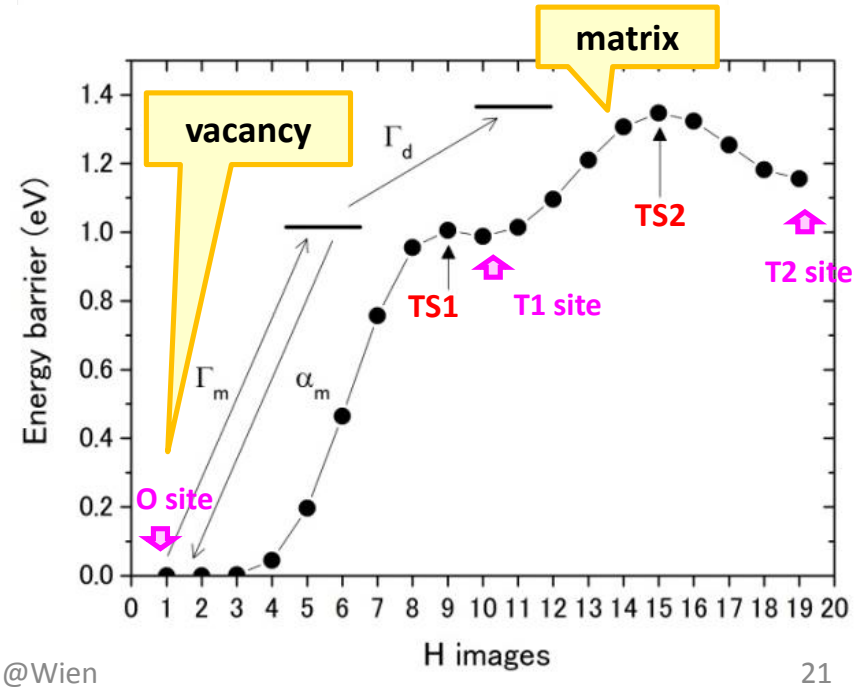

Harmonic Transition State Theory (hTST)

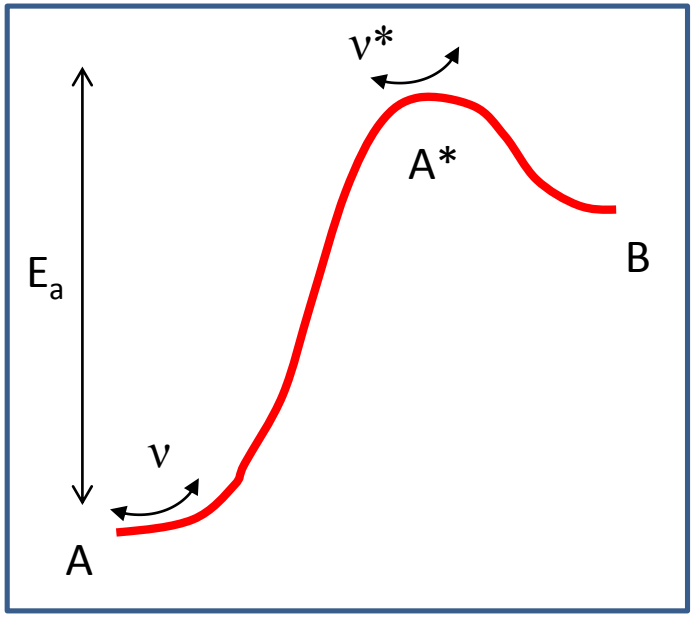

$$\mathrm{A} \Leftrightarrow \mathrm{A}^{*} \xrightarrow{\tau_{\mathrm{A}^{*}}^{-1}} \mathrm{B}$$

$$\Gamma_{\mathrm{AB}} = \tau_{\mathrm{A}^{*}}^{-1} \frac{Z_{\mathrm{A}^{*}}}{Z_{\mathrm{A}}}$$

$$= \frac{k_{\mathrm{B}}T}{h} \frac{\prod_{l}^{N} \left(1 - \exp\left(-h\nu_{l}/k_{\mathrm{B}}T\right)\right)}{\prod_{l}^{N-1} \left(1 - \exp\left(-h\nu_{l}^{*}/k_{\mathrm{B}}T\right)\right)} \exp\left(-E_{\mathrm{a}}/k_{\mathrm{B}}T\right)$$

Thermal desorption rate

$$\frac{dx_{\mathrm{A}}}{dT} = \left(\frac{dT}{dt}\right)^{-1} \frac{dx_{\mathrm{A}}}{dt} = -\alpha^{-1}\Gamma x_{\mathrm{A}}$$

$$\frac{E_{\mathrm{a}}}{k_{\mathrm{B}}T_{\mathrm{p}}^{2}} = \alpha^{-1} \frac{\prod_{l}^{N} \nu_{l}}{\prod_{l}^{N-1} \nu_{l}^{*}} \exp\left(-E_{\mathrm{a}}/k_{\mathrm{B}}T_{\mathrm{p}}\right)$$

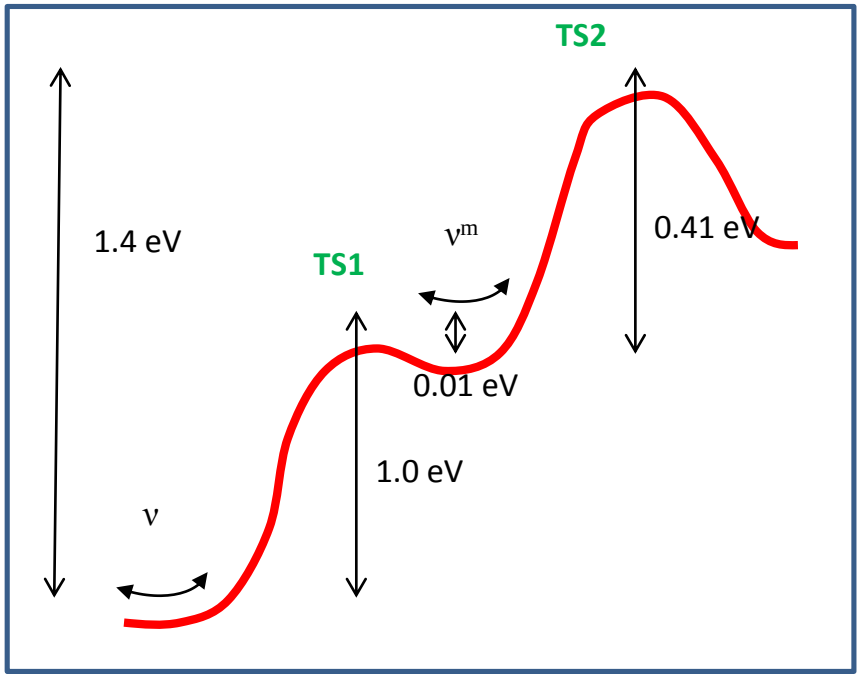

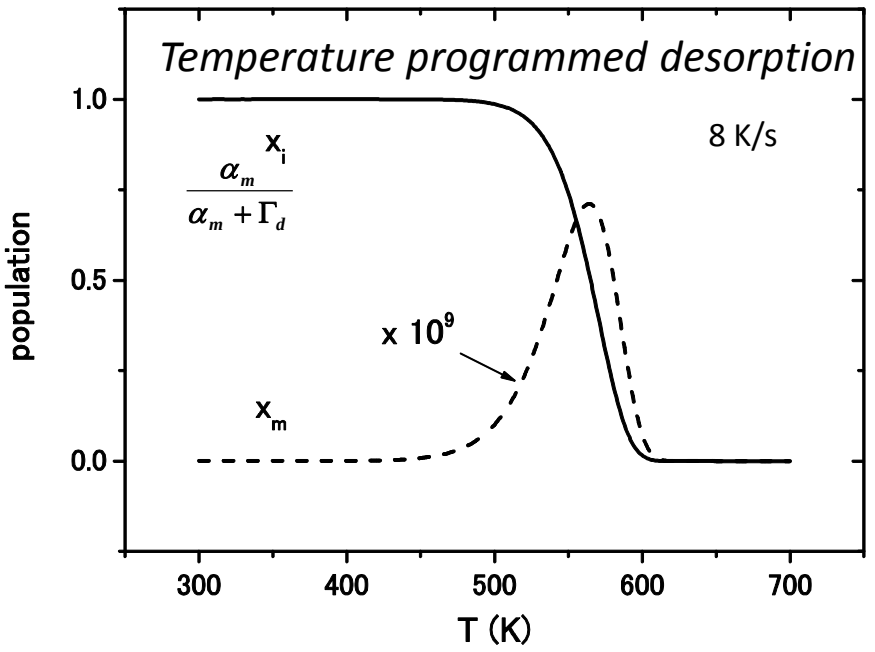

Single H desorption was calculated using transition state theories to investigate ***two-step effect***.

Branching ratio at T1 site indicates recombination dominant.

During temperature programmed desorption, population of the intermediate state (x_m) is vanishingly small and limited in a narrow temperature range.

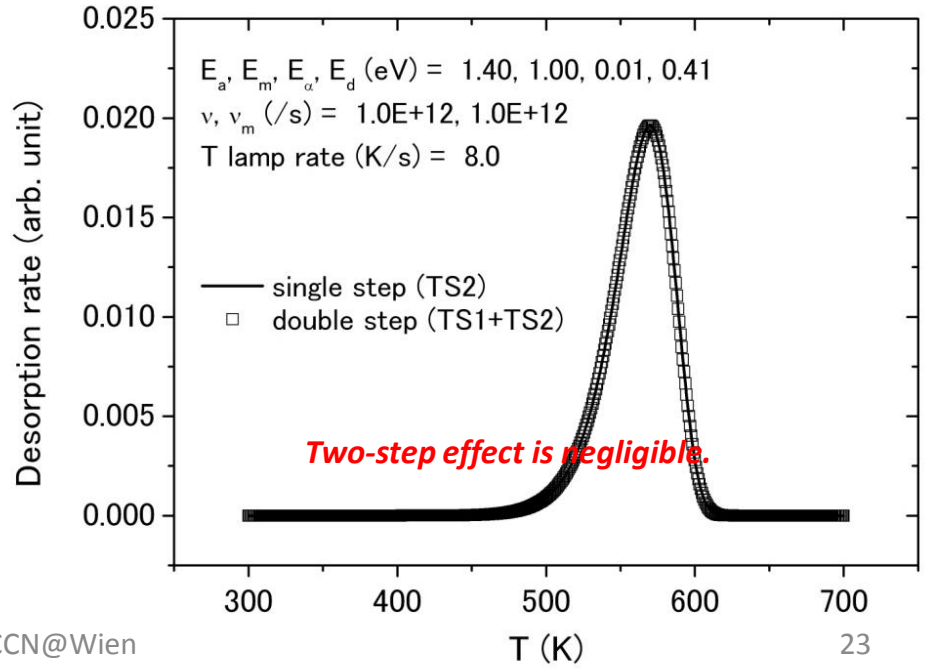

Binding energy of vacancy-hydrogen complex VH_j in W

$$e_{\mathrm{f}}(\mathrm{V}_m\mathrm{H}_j) = E(\mathrm{W}_{n-m}\mathrm{V}_m\mathrm{H}_j) - \frac{n-m}{n}E(\mathrm{W}_n) - \frac{j}{2}E(\mathrm{H}_2)$$

$$e_{\mathrm{b}}(\mathrm{H}) = e_{\mathrm{f}}(\mathrm{V}_m\mathrm{H}_{j-1}) + e_{\mathrm{f}}(\mathrm{H}) - e_{\mathrm{f}}(\mathrm{V}_m\mathrm{H}_j)$$

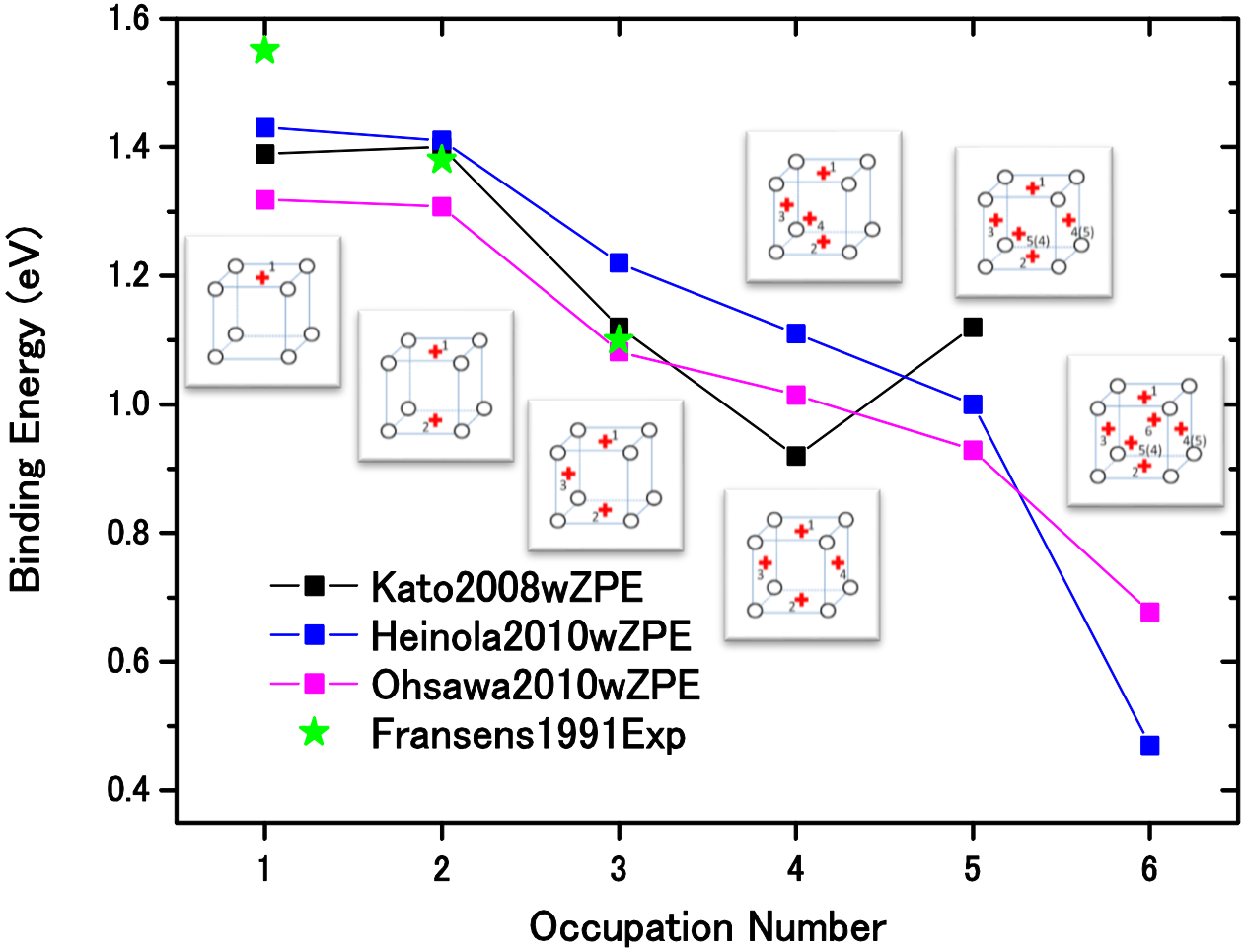

DFT calculations (solid-squares, black [Kato], blue [Heinola], pink [Ohsawa]). Experimental values by gamma-ray perturbed angular correlation of ^{111}In (stars, green). Insets show occupation sites (crosses) of hydrogen atoms in a tungsten cubic cell centered at a mono-vacancy.

Table 1. DFT results of binding energies (eV) for H in VH_j comlexes.

j	Fe	W	W ZPE	Heinola [21]	Ohsawa [22]	Exp. [25]	Exp. [26]
1	0.64	1.22	1.39	1.43	1.318	1.16(2)	0.95(3)
2	0.67	1.23	1.40	1.41	1.308	0.99(2)	0.68(3)
3	0.46	1.10	1.12	1.22	1.082		
4	0.35	0.82	0.92	1.11	1.015		
5	0.45	1.12	1.12	1	0.929	< 0.7	—
6	0.08	0.32	—	0.47	0.677		

Note: Present results [20] were obtained using a reference super-cell with 54 atoms. ZPE means the results with zero-point energy correction. Results of Heinola [21] and Ohsawa [22] include the ZPE correction. Experimental values [25] and [26] are binding energies of H in InV_2 complexes of tungsten and those of D in mono-vacancies of a D^+-irradiated single crystal tungsten, respectively (see text).

It is noted that there is still an issue regarding the maximum number of hydrogen atoms accommodated in the single vacancy. Liu and Ohsawa have suggested 10 or 12 hydrogen atoms can be accommodated in the single mono-vacancy. It has been found that with increasing occupation numbers, the trapping sites are shifted toward the tetrahedral sites.

Temperature Programmed Desorption of VH_j complex

Statistical thermodynamics model proposed by Fukai with an extension.

$$x_i = N_H / N_W, \qquad x_{V0} = \exp[-f_V / kT]$$

$$x_j \left(= N_{VH_j} / N_W\right) = \left(\frac{x_i - x_t}{6}\right)^j \omega_j \exp[-\Delta f_j / kT], \quad \omega_{0-6} = 1,6,3,4,12,6,1$$

$$x_t = \sum_j j \times x_j, \qquad x_V = \sum_{j=0} x_j$$

f : formation free energies

$$\Delta f_j = f_j - j \times f_i$$

$$f_j(T) = e_f(VH_j) + \sum_l^{3j} \left\{ \frac{h\nu_l^{(VH_j)}}{2} + kT \ln\left[1 - \exp\left(-h\nu_l^{(VH_j)} / kT\right)\right] \right\}$$

$$f_i(T) = e_f(H) + \sum_l^{3} \frac{h\nu_l^{(H)}}{2} + kT \ln\left[1 - \exp\left(-h\nu_l^{(H)} / kT\right)\right]$$

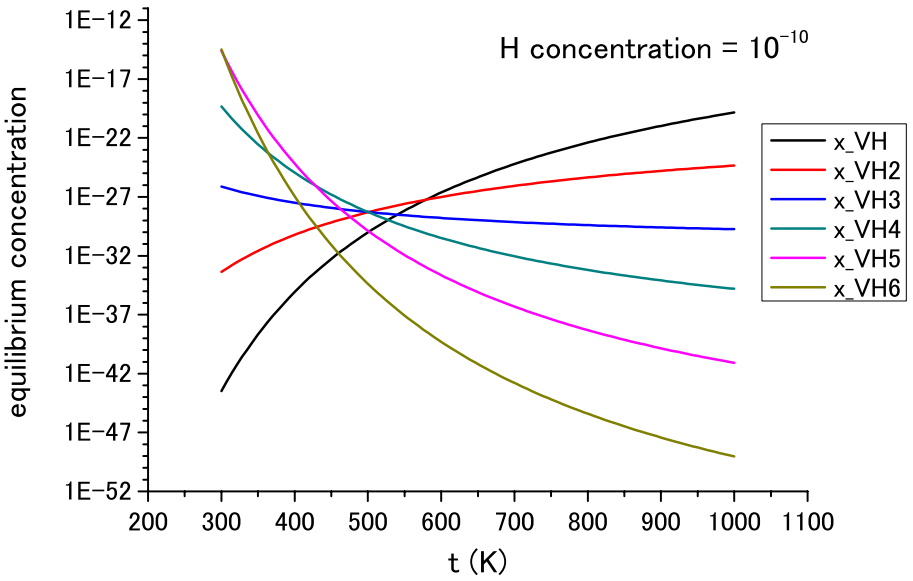

Rate equations for fractional concentrations of VH_j complexes. Desorption rates are calculated by harmonic transition state theory (hTST).

$$\begin{cases} \dfrac{dx_j}{dT} = -\alpha^{-1}\Gamma_{j\to j-1}x_j, & j = 6 \\ \dfrac{dx_j}{dT} = -\alpha^{-1}\left(\Gamma_{j\to j-1}x_j - \Gamma_{j+1\to j}x_{j+1}\right), & 1 \le j < 6 \end{cases}$$

$$\Gamma = \frac{kT}{h} \frac{\prod_l^N \left(1 - \exp\left(-h\nu_l / kT\right)\right)}{\prod^{N-1} \left(1 - \exp\left(-h\nu_l^{*TS} / kT\right)\right)} \exp\left(-E_d / kT\right)$$

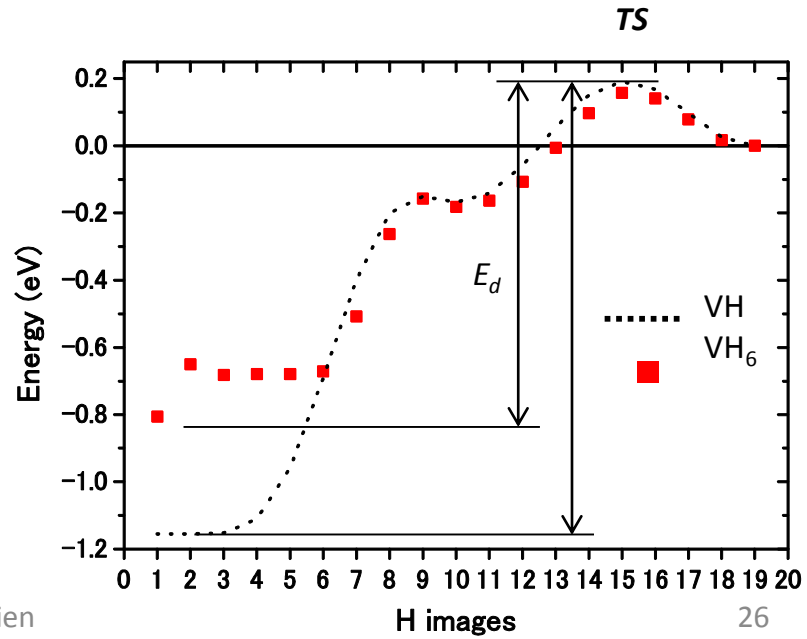

Fernandez N., Ferro Y. and Kato D. 2015 Acta Mater. 94 307

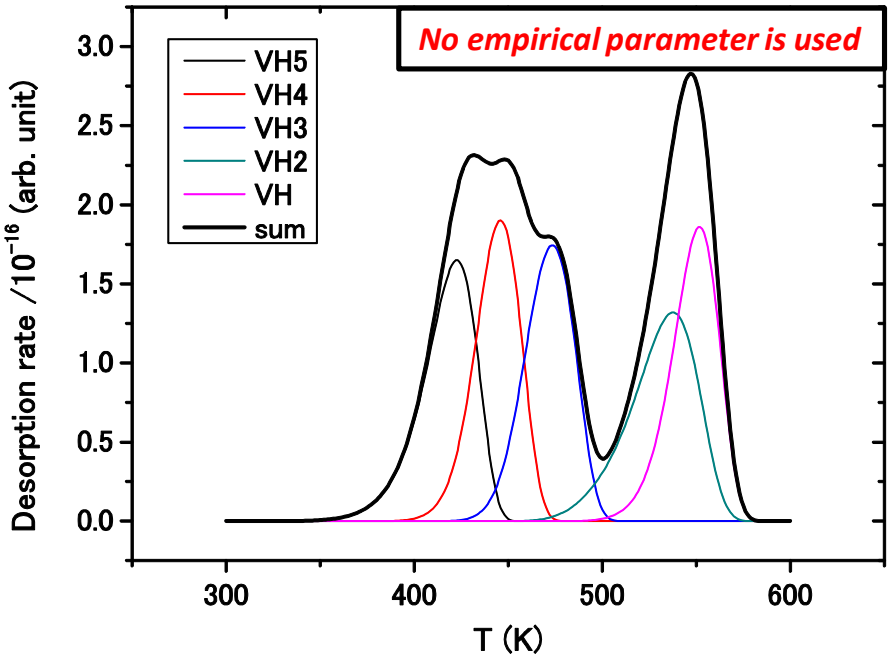

Double-peak structure is obtained. Good agreement with experimental results with SCW for higher fluence.

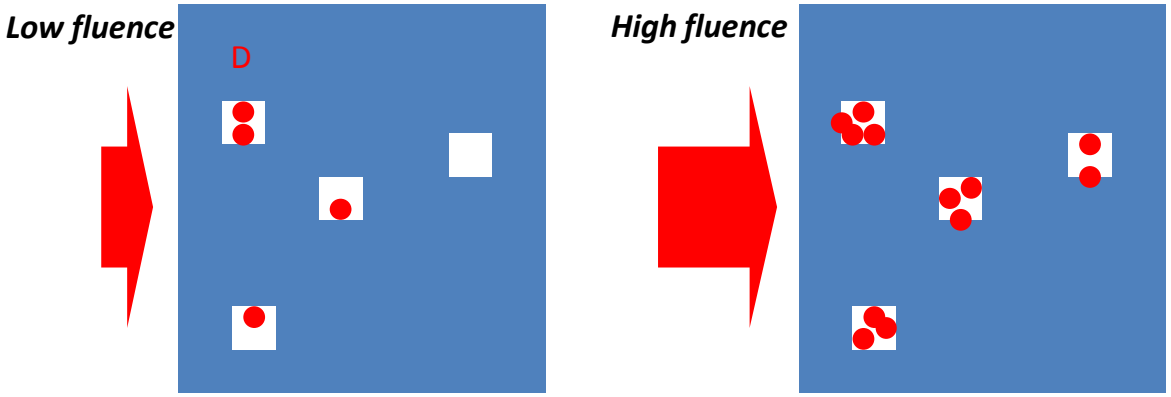

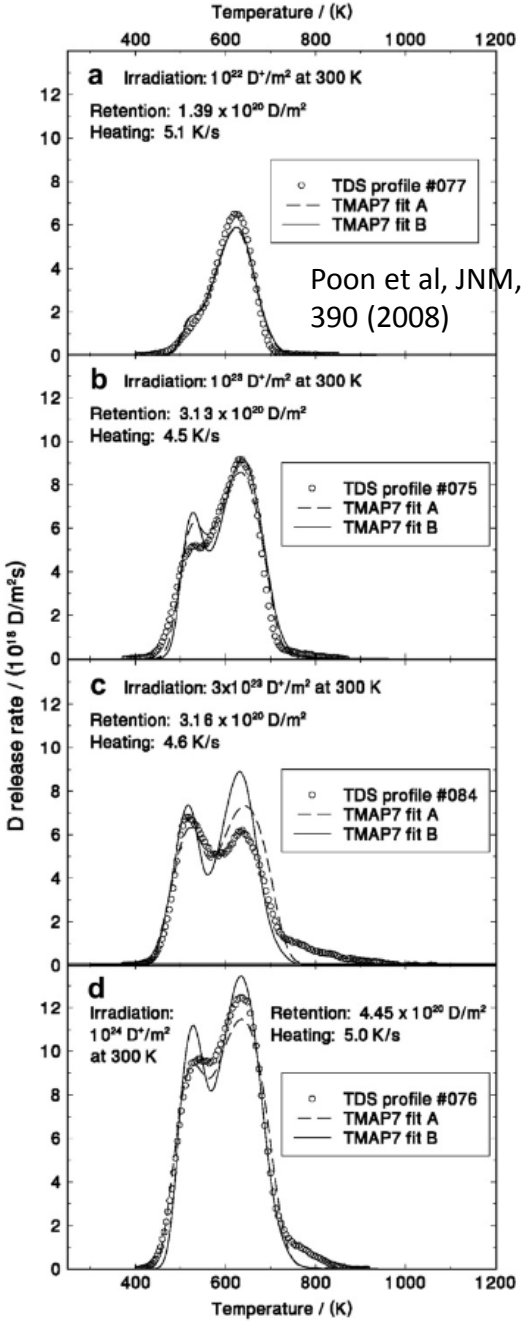

Poon et al, JNM, **374**, 390 (2008)

Summary

- Radiation damage has a primary role of tritium retention in fusion reactor plasma-facing component.
- Super-saturation of hydrogen in W divertor is anticipated. Its influence on microstructure development on the surface and tritium retention is an issue.
- DFT calculations of vacancy formation energies are improved by surface xc-energy corrections. DFT results of di-vacancy binding energies are almost zero or negative (repulsive).
- Hydrogen trapping is a clue of the abundance of di-vacancy in W (void nucleation).
- It is predicted that vacancy-hydrogen complexes can trap crowdion-SIA and suppress the vacancy-SIA annihilation.
- Detrapping of hydrogen from vacancy-hydrogen complexes are investigated based on the hTST using DFT energies and normal mode frequencies. Reasonable agreement with experimental measurements. Similar analysis will be performed for larger complexes.

UQ issues for modeling

- Numerical convergence of DFT calculations, e.g. k-point sampling and smearing, plane-wave energy-cutoff, super-cell size, energy-functional (especially for surface), pseudo-potential.
- Characterization of hydrogen traps in the model.
- How to scale-up the DFT results for larger systems, e.g. potential development for MD, parameter passing for KMC, statistical scaling (thermodynamics, CE)

Acknowledge

This work is supported by Zero emission "Joint Usage/Research Program on Zero-Emission Energy Research, Institute of Advanced Energy, Kyoto University (ZE26A-8). DK thanks to NIFS/NINS under the project of Formation of International Scientific Base and Network.

A part of this work was carried out using the HELIOS supercomputer system at Computational Simulation Centre of International Fusion Energy Research Centre (IFERC-CSC), Aomori, Japan, under the Broader Approach collaboration between Euratom and Japan, implemented by Fusion for Energy and JAEA.